

Efficiency enhancement in plasmonic dye-sensitized solar cells with TiO₂ photoanodes incorporating gold and silver nanoparticles

M. A. K. L. Dissanayake^{1,2} · J. M. K. W. Kumari^{1,2} · G. K. R. Senadeera^{1,2,3} · C. A. Thotawatthage^{1,2}

Received: 11 May 2015 / Accepted: 24 August 2015 / Published online: 3 September 2015
© Springer Science+Business Media Dordrecht 2015

Abstract Plasmonic dye-sensitized solar cells (DSSCs) were fabricated using TiO₂ photoanodes incorporating gold nanoparticles (AuNPs) with 15–20-nm size and silver nanoparticles (AgNPs) with 40–60-nm size. These were characterized by UV–Vis spectroscopy, *J*–*V* characteristic, IPCE spectroscopy, EIS analysis and dark *I*–*V* measurements. Under the illumination of 100 mW cm⁻² (AM 1.5), the efficiency of the reference DSSC without Au and Ag NPs in TiO₂ was 5.12 %, while the efficiencies of plasmonic DSSCs with TiO₂:AuNP and TiO₂:AgNP were 6.23 and 6.51 %, respectively, representing an efficiency enhancement by 21.6 % for AuNPs and 27 % for AgNPs. The increased efficiencies of the two plasmonic DSSCs appear to be due to the increased short-circuit photocurrent density by enhanced light harvesting caused by the localized surface plasmon resonance effect. The IPCE spectra of the two plasmonic DSSCs suggest the narrowing of the energy band gap of TiO₂ due to the presence of Au and Ag nanoparticles.

Keywords Dye-sensitized solar cells · Efficiency enhancement · TiO₂ photoanodes · Gold and silver nanoparticles · Surface plasmon resonance effect

1 Introduction

Since the dye-sensitized solar cell (DSSC) was first reported by Grätzel et al. [1], it has been a focus of intensive research activity aimed at developing low-cost, high-performance solar cells. In the past few decades, this has been achieved largely by developing better sensitizers [2–4], novel electrolytes and improved photoanodes [5–9]. Recently, some unconventional approaches for enhancing dye-sensitized solar cell performance have also been actively demonstrated. In particular, the effect of surface plasmons, arising from noble metal nanoparticles (such as Au and Ag), has been used to increase the optical absorption and photocurrent in plasmonic DSSCs [10–15].

Gold and silver nanoparticles have been extensively used for applications both in biology (e.g., bio-imaging) and technology (e.g., photonics) due their unique optical properties. These properties are conferred by the interaction of light with electrons on the nanoparticle surface. At a specific wavelength of light, collective oscillations of electrons on the nanoparticle surface cause a phenomenon called Local Surface Plasmon Resonance (LSPR) resulting in strong extinction of light (absorption and scattering). The particular wavelength, or frequency, of light where this occurs is strongly dependent on the nanoparticle type, size, shape, surface, and agglomeration state. The surface plasmon resonance effect is manifested by the constructive interference between electromagnetic light fields and the surface plasmons of metal NPs. The LSPR effect amplifies and intensifies the electromagnetic fields near the metal NPs, leading to the precise control of optical fields and the enhanced absorption band in the UV–Vis spectrum. The use of the plasmonic effect for light trapping, therefore, provides an efficient way to make the full use of the dyes for enhancing solar cell efficiency.

✉ M. A. K. L. Dissanayake
makldis@yahoo.com

¹ National Institute of Fundamental Studies, Kandy, Sri Lanka

² Postgraduate Institute of Science, University of Peradeniya, Peradeniya, Sri Lanka

³ Department of Physics, The Open University of Sri Lanka, Nawala, Nugegoda, Sri Lanka

In the case of DSSCs, Ihara et al. demonstrated an enhanced absorption coefficient of the Ru-dye using an Ag island film [16]. Jeong et al. investigated the photocurrent improvement due to the increased effective absorption cross section of the dye as a result of the neighboring Ag NPs [17]. More recently, various plasmonic structures have been used to increase the photovoltaic (PV) performance of DSSCs [18–21]. Extending the LSPR effect further, plasmon-enhanced light absorption of the dye and hence the increased photocurrent have been demonstrated in DSSCs by incorporating metal (Au, Ag) particles and more often by introducing the metal@TiO₂ [22], metal@SiO₂ [23], or metal@SiO₂@TiO₂ core-shell structures [24] into flat or porous TiO₂ anode.

In the present study, Au and Ag NPs were synthesized using conventional citrate reduction method and incorporated into TiO₂ photoanode. The volume effects of Au and Ag NPs on the PV performance of the plasmonic DSSCs were studied in detail. The UV–Vis absorption spectra and incident photon to current conversion efficiency (IPCE) spectra were measured. The results of the electrochemical impedance spectroscopy (EIS), Dark I–V characteristics, and Flat Band Potential measurements were analyzed to support the short-circuit current density enhancement caused by the surface plasmon effect in the plasmonic DSSCs.

2 Experimental

2.1 Preparation of gold and silver nanoparticle suspensions

Au and Ag nanoparticles can be synthesized using the citrate reduction method. According to the literature, this method produces gold NPs with diameters ranging from 15 to 20-nm and relatively larger-sized silver nanoparticles with diameters ranging from 40 to 60 nm. In this study, gold nanoparticles were prepared following the procedure described by Tabrizi et al. [25] and Huang et al. [26]. Hydrogen tetrachloroaurate (III) and trisodium citrate purchased from Fluka were used as starting materials. A 20-ml solution of 1 mM of H₂AuCl₄ was prepared by adding distilled water, and the solution was boiled under continuous stirring. 1 % Na₃C₆H₅O₇ solution was prepared by dissolving 0.1 g of the salt in 10 ml of distilled water. 2 ml of this solution was added to the boiling solution of H₂AuCl₄. The color of the solution mixture gradually changed from blue to deep red. The heating was stopped when the solution has turned deep red (Fig. 1). The mechanism of the chemical reaction could be expressed as follows:

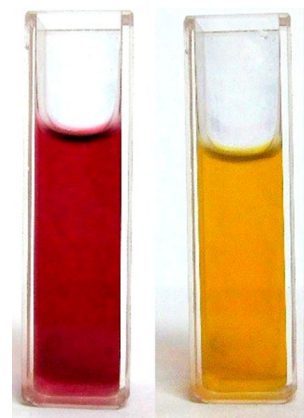
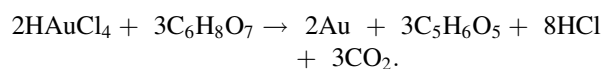
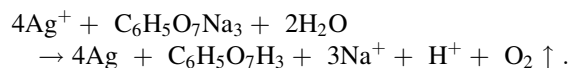


Fig. 1 Photographs of (a) Colloidal Au NPs (deep red color) and (b) Colloidal Ag NPs (orange color) prepared in this work. (Color figure online)



Silver nanoparticles were prepared following the procedure described by Chang et al. [27] and Ratyakshi et al. [28]. Silver nitrate was purchased from BDH and trisodium citrate was purchased from Fluka. 1 mM of AgNO₃ 25 ml solution was prepared by adding distilled water and the solution was boiled with continuous stirring. 1 % Na₃C₆H₅O₇ solution prepared by dissolving 0.1 g in 10 ml of distilled water and 2.5 ml of this solution was added to the boiling solution of AgNO₃. The solution mixture gradually changed from colorless to yellow. The heating was stopped when the solution has turned yellow (Fig. 1). The mechanism of the chemical reaction could be expressed as follows:



2.2 Optical absorption measurements on colloidal solutions

Optical absorption spectra of the Au NP and Ag NP colloidal solutions were taken with a Shimadzu 2450 UV–Vis spectrophotometer in the wavelength range from 300 nm to 800 nm.

2.3 TiO₂ electrode preparation and characterization

Nanocrystalline TiO₂ photoelectrodes were prepared by using the following procedure. 0.20 g of TiO₂ powder (Degussa P-25) was ground for 30 min with 12 drops (about 0.15 g) of glacial acetic acid, one drop (about 0.02 g) of Triton X-100 and about 2 ml of ethanol until the mixture became a creamy paste. Appropriate amounts of

Au nanoparticle colloidal suspension (by volume) were added to the TiO₂ paste and ground again for 15 min to obtain a homogeneous material. The same procedure was repeated by adding Ag nanoparticle colloidal suspension to obtain TiO₂ paste with Ag nanoparticles. The paste was doctor bladed on a precleaned Fluorine-doped conducting Tin Oxide (FTO) glass (Solaronix sheet glass 8 Ω/sq) keeping the active cell area of 0.25 cm². In order to compare the effects of Au and Ag nanoparticles in the TiO₂ films, pristine TiO₂ films were also prepared without adding Au and Ag nanoparticles. FTO/TiO₂ plates were sintered at 450 °C for 45 min and slowly cooled down to room temperature. They were subsequently dipped in an ethanolic dye (0.3 M) solution containing Ruthenium dye N 535 [RuL₂ (NCS)₂: 2TBA where, L = 2,2'-bipyridyl-4', dicarboxylic acid; TBA = tetrabutyl ammonium] for 24 h [5].

The XRD spectra of the TiO₂, TiO₂ Au NP, and TiO₂ Ag NP were taken in order to confirm the presence of Au NPs and Ag NPs in the respective plasmonic photoanodes.

2.4 Plasmonic solar cell fabrication and I–V characterization

The electrolyte solution for the DSSCs was prepared by adding 0.738 g of tetrapropyl ammonium iodide (Pr₄NI) and 0.060 g of I₂ to a precleaned 10-ml volumetric flask containing 3.6 ml of molten (MP 40 °C) ethylene carbonate (EC) and 1.0 ml of acetonitrile. The solution mixture was stirred overnight. DSSCs were fabricated by sandwiching the above electrolyte solution containing I⁻/I₃⁻ redox couple in the configuration FTO/TiO₂/dye/electrolyte/Pt/FTO. The photocurrent–voltage (I–V) characteristics of the cells were measured under the illumination of 100 mW cm⁻² (AM 1.5) simulated sunlight using a homemade computer-controlled setup coupled to a Keithley 2000 multi-meter and a potentiostat/galvanostat HA-301. A Xenon 500 W lamp was used with AM 1.5 filter to obtain the simulated sunlight with above intensity.

2.5 Flat band potential measurement

Flat band potential of the photoanodes can be used to understand the movement of the Fermi Level of the metal NP-incorporated TiO₂ electrodes with respect to the reference photo electrode. In order to find the flat band potential of the three TiO₂ electrodes, Mott-Schottky measurements were taken by immersing TiO₂, TiO₂-Au NP, and TiO₂-Ag NP electrodes in a 0.5 M Na₂SO₄ electrolyte solution, one at a time. The stabilized voltage was measured with respect to a standard calomel electrode (SCE) using a Metrohm Autolab PGSTAT 128 N

potentiostat. The scanned frequencies were 1.0 kHz and 2.0 kHz.

2.6 IPCE and optical absorption measurements

IPCE is defined as the number of electrons in the external circuit produced by an incident photon at a given wavelength divided by the number of incident photons. IPCE measurements were taken for the above three DSSC systems, (A) TiO₂/dye/liquid electrolyte/Pt, (B) TiO₂-Au NP/dye/liquid electrolyte/Pt, and (C) TiO₂-Ag NP/dye/liquid electrolyte/Pt. Experimental setup consisted of monochromatic light illumination from a Bentham PVE300 unit equipped with a TMC 300 monochromator-based IPCE system with a 150 W xenon arc lamp covering the 300–800-nm wavelength range. A calibrated Si photo detector (type DH) was used as the reference. For comparison purposes, the UV–Vis absorption spectra of the metal NP incorporated TiO₂ powder samples of the three dyed photoanode materials was also taken. For these measurements, a paste of (a) TiO₂, (b) TiO₂-Au NP, or (c) TiO₂-Ag NP was applied on FTO glass plate. After sintering at 450 °C for 45 min., the powder was scratched off from glass plates. 0.1 g of each powder was dipped in 2 ml of Ru dye solution. After leaving for 24 h for dye loading, these dyed powder samples were washed and dried, and then used to get the optical absorption curves. UV–Vis Absorption spectrum was also taken for powder samples of TiO₂, TiO₂-Au NP, and TiO₂-Ag NP without dye for the determination of the corresponding energy band gap values. All optical absorption measurements were done using a Shimadzu 2450 UV–Vis spectrophotometer in the wavelength range of 300–800 to nm.

2.7 EIS measurements

In order to see the effects of metal NP-incorporated TiO₂ on the electron life time and the interfacial charge-transfer resistance, R_{2CT} , electrochemical Impedance Spectroscopy (EIS) measurements were performed on the DSSCs using a Metrohm Autolab Potentiostat/Galvanostat PGSTAT 128 N with a FRA 32 M Frequency Response Analyzer (FRA) covering the 1 MHz–0.01 Hz frequency range. These measurements were carried out under the illumination of 100 mW cm⁻² using the same solar simulator that was used for I–V measurements.

2.8 Dark I–V measurements

Dark I–V measurements were performed for the three different types of DSSCs using Autolab PGSTAT 128 N in order to see the effect of metal NP-incorporated TiO₂ on the reverse breakdown voltage of the DSSCs.

3 Results and discussion

3.1 Optical absorption by gold and silver nanoparticles' colloidal suspensions

The colloidal suspensions of gold NPs and silver NPs prepared in this study exhibit a deep red color and an orange color, respectively, as shown in Fig. 1. The UV–Vis optical absorption spectra of the two metal NPs' colloidal suspensions are shown in Fig. 2. As seen from Fig. 2, the absorption spectra of the Au and Ag colloids exhibit a surface plasmon absorption band with the maxima around 520 and 420 nm, respectively. From the positions of these absorption maxima, it has been estimated that the diameters of the gold nanoparticles are in the 15–20-nm range [29], and the diameters of the silver nanoparticles are in the 40–60-nm range [30].

As the sizes or the shapes of the nanoparticles change, the observed color also changes. Gold nanospheres prepared in this work have a characteristic red color, while the silver nanospheres are orange as shown in Fig. 1. It is generally accepted that the color is due to the collective surface plasmon oscillations of the electrons in the conduction band. The oscillation frequency is usually in the visible region for gold and silver giving rise to the strong surface plasmon resonance absorption [31]. Although the conduction and valence bands of semiconductors such as TiO_2 are separated by a well-defined band gap, metal nanoparticles have close-lying bands where electrons can move quite freely. These free electrons give rise to surface plasmon-absorption bands in metal NPs, which depends on both the particle size and the chemical surroundings.

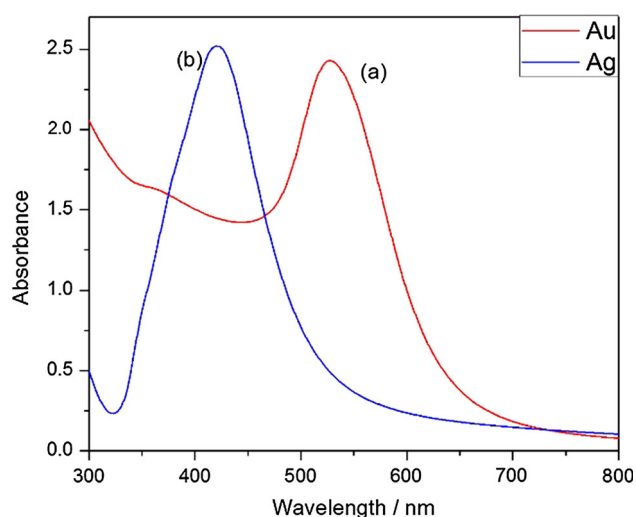


Fig. 2 Absorbance spectra of (a) Colloidal Au NPs and (b) Colloidal Ag NPs. (Color figure online)

The free electrons in the metal (d electrons in Au and Ag) are free to travel through the material. The mean free path in Au and Ag is nearly 50 nm, and therefore, in particles smaller than this, no scattering is expected from the bulk [31]. Thus, all interactions are expected to be within the surface. When the wavelength of light is much larger than the nanoparticle size, it can set up standing resonance conditions. Light in resonance with the surface plasmon oscillation causes the free-electrons in the metal to oscillate. As the wave front of the light passes, the electron density in the particle gets polarized to one surface and oscillates in resonance with the light's frequency causing a standing oscillation. Under this surface plasmon resonance condition, enhanced light absorption occurs which depends on the types, sizes, shapes, and the dielectric constants of the metal and the surrounding medium.

3.2 Optimization of DSSC efficiency by incorporating different amounts of Gold and Silver NP suspensions into TiO_2 electrodes

Different amounts (M_{Au} , moles) of gold NP colloidal suspension were added while preparing the TiO_2 paste, and plasmonic DSSCs were fabricated as described in Sect. 2.4 using TiO_2 Au NP and TiO_2 Ag NP photoanodes, and their efficiencies were determined from I–V characteristics (Tables 1).

The XRD patterns of the TiO_2 , TiO_2 -Au NP, and TiO_2 -Ag NP powders, taken after sintering are shown in Fig. 3. Although the peak intensity due to the NPs are very

Table 1 Efficiency variations with the added amounts of gold NPs (left) and silver NPs (right)

$M_{\text{Au}}/(\times 10^{-7} \text{ mol})$	$\eta \%$
0.00	5.00 ± 0.09
1.09	5.22 ± 0.05
1.81	5.47 ± 0.07
2.36	5.84 ± 0.02
2.72	5.59 ± 0.08
3.27	5.35 ± 0.02
$M_{\text{Ag}}/(\times 10^{-7} \text{ mol})$	$\eta \%$
0.00	5.00 ± 0.09
1.27	5.24 ± 0.06
2.00	5.34 ± 0.04
2.45	5.82 ± 0.03
2.91	6.12 ± 0.07
3.36	5.38 ± 0.04
3.82	5.05 ± 0.04

The bold numbered rows correspond to the DSSCs with highest efficiency

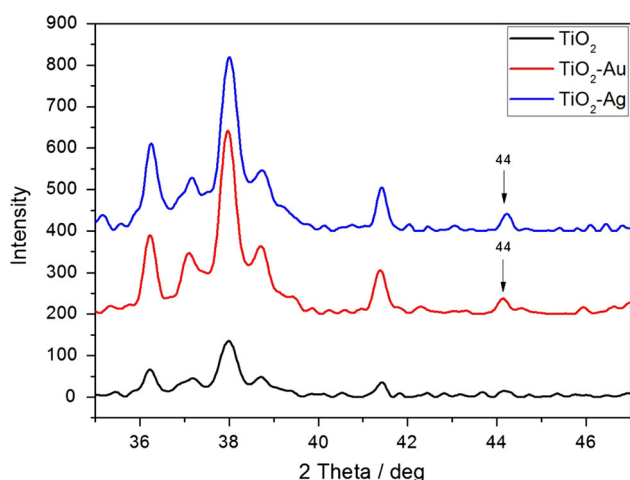


Fig. 3 XRD spectra of pristine TiO₂, TiO₂ Au NP- and TiO₂ Ag NP-sintered powders. (Color figure online)

weak and most of the characteristic peaks of both Au NPs and Ag NPs overlap with peaks of the pristine TiO₂ (P25) powder, the weak peaks at 2 theta = 44° gives clear evidence for the presence of the Au and Ag nanoparticles.

Figure 4 shows the efficiency variations with the number of moles of gold and silver NPs incorporated into TiO₂ in the plasmonic DSSCs. In each case, the efficiency vs the amount of metal NPs goes through a maximum, and the highest efficiency values are obtained for DSSCs with $M_{Au} = 2.36 \times 10^{-7}$ mol and $M_{Ag} = 2.91 \times 10^{-7}$ mol, respectively. The initial increase in the efficiency is clearly due to the enhanced light absorption by the electrons in the metal NPs due to local surface plasmon resonance effect which is proportional to the number of metal NPs incorporated into TiO₂ electrode. This increases the short-circuit photocurrent density, J_{sc} of the two plasmonic DSSCs and hence their efficiencies. Concurrently, a competing mechanism starts to dominate when the amount of incorporated

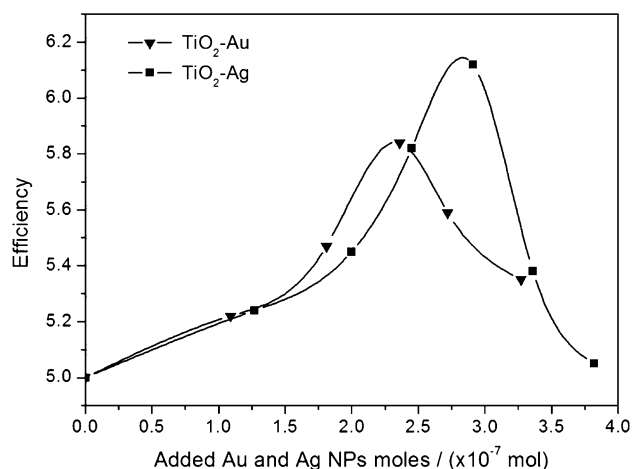


Fig. 4 Variations of efficiency of DSSCs with the amounts of gold and silver NPs incorporated into TiO₂ photoanodes

metal NPs increases. A large number of these NPs could concentrate inside the TiO₂ crystallites rather than arranging them in the surface of TiO₂ crystallites and thereby increase the parasitic absorption, which does not generate an electron/hole pair. This parasitic absorption significantly hampers the plasmonic effect and eventually decreases the photocurrent and the efficiency of the DSSC after reaching to a maximum favorable incorporation of NPs [32].

3.3 Photovoltaic performance of DSSCs

The comparison of photocurrent density versus voltage (I–V) curves for the three types of DSSCs with photoanodes (A) TiO₂ only, (B) TiO₂ with Au NPs, and (C) TiO₂ with Ag NPs under the same illumination conditions is shown in Fig. 5. For these of DSSCs, the fill factor (*FF*) is calculated using Eq. (1), and the overall energy conversion efficiency (η) was estimated using Eq. (2). In Eq. (1), the V_m and J_m are the voltage and the current density, respectively, for the maximum power output;

$$FF = J_m V_m / J_{sc} V_{oc} \tag{1}$$

$$\eta = J_{sc} V_{oc} FF / \text{Total incident power density} \tag{2}$$

The short-circuit photocurrent density, J_{sc} open-circuit voltage, V_{oc} , the fill factor, *FF*, and the efficiency, η , derived from photo current–voltage measurements (Fig. 4)

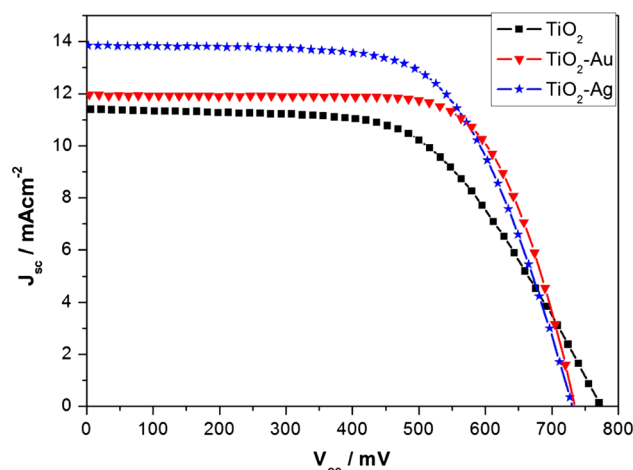


Fig. 5 Photocurrent density–voltage curves for DSSCs with (a) normal TiO₂, (b) TiO₂–Au NP, and (c) TiO₂–Ag NP. (Color figure online)

Table 2 Photovoltaic parameters of the DSSCs with (A) TiO₂, (B) TiO₂–Au NP, and (C) TiO₂–Ag NP

DSSC photoanode	J_{sc} (mA cm ⁻²)	V_{oc} (mV)	<i>FF</i> (%)	η (%)
(A) TiO ₂	11.36	771.3	58.42	5.12
(B) TiO ₂ –Au NP	12.00	737.3	70.66	6.23
(C) TiO ₂ –Ag NP	13.86	729.1	64.37	6.51

of the three types of DSSCs are summarized in the Table 2. When preparing these DSSCs, it was ensured to have the same TiO₂ film thickness of $\sim 5 \mu\text{m}$ and the same amount of dye loading.

When the photovoltaic parameters of the three DSSCs A, B, and C shown in Table 2 are compared, one can clearly see that the short-circuit photocurrent density (J_{sc}), the fill factor (FF), and the energy conversion efficiency (η) values of the B and C plasmonic DSSCs have increased, but their open-circuit voltage (V_{oc}) values have decreased.

As seen from Table 2, the conversion efficiency for DSSCs made with pristine TiO₂, TiO₂-Au NP, and TiO₂-Ag NP are 5.12, 6.23, and 6.51 %, respectively, showing clearly that the enhanced short-circuit photocurrent density, J_{sc} in the two plasmonic DSSCs is largely responsible for the enhanced efficiency in these cells. The photocurrent density enhancement evidently takes place due to the improved light absorption by the metal NP containing TiO₂ electrode in the two plasmonic DSSCs by the local plasmon resonance effect as already described in the Introduction section. The overall solar cell efficiency has shown a dramatic increase by 21.6 % for the solar cells with Au NPs and by 27.1 % for the solar cells with Ag NPs. However, it should be noted that the V_{oc} values of the two plasmonic DSSCs have decreased relative to the reference DSSC. A possible mechanism for this effect will be discussed later after the IPCE spectra and results of the Flat Band Potential measurements are analyzed. Clearly, the contributions from the enhancement in J_{sc} to the overall energy conversion efficiency of the two plasmonic DSSCs grossly outweigh the reduction in V_{oc} resulting in the observed efficiency enhancement. Very similar results of enhanced J_{sc} values due to plasmon-induced charge transfer are reported for the plasmonic DSSCs incorporating Ag nanoparticles in TiO₂ nanofiber-based photoanodes [33].

3.4 IPCE analysis

The effectiveness of a dye-sensitized cell to convert light of various wavelengths into electrical energy is measured by the incident monochromatic light current conversion efficiency (IPCE) defined as the number of electrons generated by light per number of photons incident on the cell as formulated by $\text{IPCE} \% = 1240 J_{\text{sc}}/\lambda W_i$ where J_{sc} is the short-circuit current density (mA cm^{-2}), λ the excitation wavelength (nm), and W_i is the photon flux (W m^{-2}).

Results of IPCE measurements taken for the three DSSC systems: (A) TiO₂/dye/liquid electrolyte/Pt, (B) TiO₂-Au NP/dye/liquid electrolyte/Pt, and (C) TiO₂-Ag NP/dye/liquid electrolyte/Pt, using Ru N719 as the sensitizing dye, are shown in Fig. 6. The IPCE peak height for TiO₂-Ag DSSC is 56.1 % at 539 nm, and for TiO₂-Au NP DSSC, it is 52.4 % at 533 nm. Both these are much higher than the

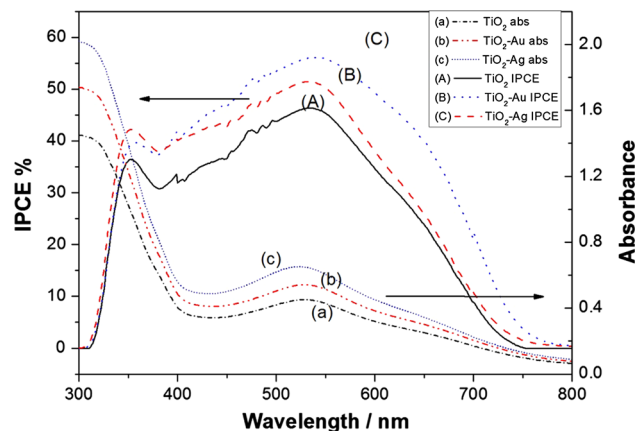


Fig. 6 Comparison of optical absorption curves for sintered and dyed powders (a) TiO₂-dye, (b) TiO₂-Au NP-dye, and (c) TiO₂-Ag NP-dye; and spectral responses (IPCE) of DSSCs with photoanodes: (A) TiO₂, (B) TiO₂-Au, and (C) TiO₂-Ag. (Color figure online)

peak height of 46.3 % at 531 nm for reference TiO₂ DSSC. The UV-Vis absorption spectra of the metal NP-incorporated, sintered, and dyed TiO₂ powder samples of the three photoanode materials: (a) TiO₂-dye, (b) TiO₂-Au NP-dye, or (c) TiO₂-Ag NP-dye are also shown in the same figure for easy comparison with IPCE spectra.

There are two major effects that can be expected due to the presence of the Au and Ag NPs in TiO₂ photoelectrodes: (1) increased light absorption due to surface plasmon effect as described earlier under the Introduction; and (2) narrowing of the energy band gap in metal NP-incorporated TiO₂ electrodes. We can observe the results of both these effects in the IPCE spectra of the two plasmonic DSSCs.

As seen from Fig. 6, the amounts of absorption by all the wavelengths in the visible region as estimated from the total integrated area under the absorption curve also increases substantially from 0.45 (Reference TiO₂ powder) to 0.54 (TiO₂-Au NP powder) and to 0.65 (TiO₂ Ag NP powder) (Table 3). This supports the absorption enhancement by plasmon resonance effect in the two plasmonic solar cells. The strongly localized electromagnetic field around the Au and Ag NPs will strongly enhance the optical absorption efficiency of the dye molecules, resulting in the observed increase in the photocurrent of the Au and Ag NP-incorporated DSSC systems [15, 33]. Therefore, apart from the electron injection from the dye molecules due to the photoexcitation, the gold and silver nanoparticles are also photoexcited due to the plasmon resonance effect, and charge separation is accompanied by the transfer of photoexcited electrons from the metal particle to the TiO₂ conduction band and the simultaneous transfer of compensative electrons from the donor in the electrolyte to the metal particle.

As can be seen from the figure, there is a good agreement between the wavelength maxima in the IPCE plots

Table 3 Wavelengths of the maxima in the powder absorption spectra and the maxima of the IPCE spectra of the reference DSSC and the DSSCs with Au and Ag NPs. Data taken from Fig. 5

Powder sample used for photoanode	Absorbance peak (nm)	Absorption (Relative)	DSSC	IPCE peak wavelength (nm)
(a) TiO ₂ -dye	528	0.45	(A) TiO ₂	531
(b) TiO ₂ -Au-dye	527	0.54	(B) TiO ₂ -Au	533
(c) TiO ₂ -Ag-dye	522	0.65	(C) TiO ₂ -Ag	539

(IPCE_{max}) of these three DSSC systems and the dye absorption maxima (Abs_{max}) of the corresponding dyed TiO₂ anode powders. For the reference D-TiO₂ system, the IPCE_{max} (=531 nm) is slightly red shifted from Abs_{max} (=528 nm). For D-TiO₂-Au NP plasmonic system, the IPCE_{max} (=533 nm) is red shifted from Abs_{max} (=527 nm) and for D-TiO₂-Ag NP plasmonic system, the IPCE_{max} (=539 nm) is also red shifted from Abs_{max} (=522 nm). This phenomenon was described by Standridge et al. [11] where it was observed that the red shift in the IPCE_{max} occurs relative to D-TiO₂ (powder) system when Au and Ag NPs were incorporated. Similar behavior was reported for solar cells containing Au NPs by Hagglund et al. [31, 32] and for solar cells containing Ag NPs by Rand et al. [33].

The observed red shift in the IPCE_{max} of the two plasmonic DSSCs can be easily understood by referring to the apparent Fermi level shift obtained from Mott-Schottky measurements as discussed below under the flat band potential.

3.5 Flat band potential analysis

Results of the flat band potential measurements of the three types of TiO₂ electrodes are shown in Fig. 7. This figure clearly shows the reduction in the flat band potential V_{fb} values of the TiO₂ Au NP and TiO₂ Ag NP electrodes

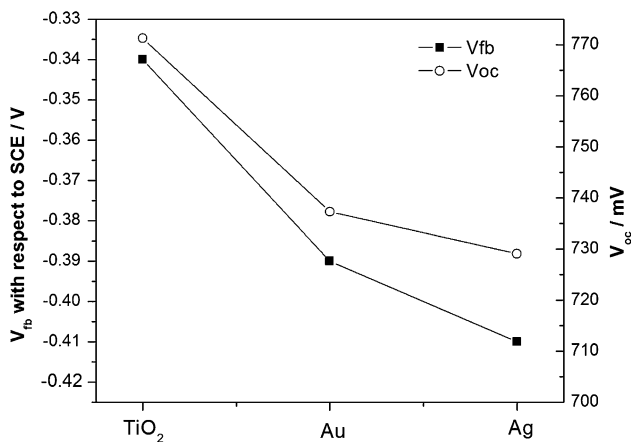


Fig. 7 Flat band potential (V_{fb}) values of the three different photoelectrodes: (a) Reference TiO₂, (b) TiO₂ Au NP, and (c) TiO₂ Ag NP and their comparison with V_{oc} values of the three corresponding DSSCs

compared to that of reference TiO₂ electrode, in agreement with the observed reduction of the V_{oc} following the same trend.

In a DSSC kept in the dark, the Fermi level equilibrates with the redox couple present in the electrolyte. Upon excitation of TiO₂ films by light, one observes a rise in the photovoltage as the electrons accumulate within the TiO₂ film. As the semiconductor TiO₂ and metal NP are in contact, the photogenerated electrons are distributed between TiO₂ and metal NPs. The transfer of electrons from the excited TiO₂ into metal NPs continues until the two systems attain equilibrium. This electron accumulation shifts the resultant pseudo Fermi level (E'_F) of the composite system (TiO₂ and metal NPs) to more negative values. When this happens, the system attains a new photo equilibrium. For an intrinsic semiconductor, the value of E'_F is given by the expression:

$$E'_F = E_{CB} + kT \ln(n_c/N_c)$$

where E_{CB} is conduction band energy, N_c is the effective state density, and n_c is the carrier density including the accumulated electrons [32]. Therefore, the position of the pseudo Fermi level E'_F will depend on both the position of ECB and the total concentration of electrons in the TiO₂. Any shift in E'_F thus represents increased accumulation of electrons in the TiO₂ film. The magnitude of the photovoltage (V_{oc}) represents the energy difference (ΔE) between the apparent Fermi level (E'_F) of the TiO₂ film and the reduction potential (E°_{redox}) of the redox couple in the electrolyte,

$$V_{OC} = \Delta E = E'_F - E^{\circ}_{redox}$$

According to the results of our flat band potential measurements (Fig. 7), the apparent Fermi level (E'_F) has shifted to more negative values for the two metal NP-incorporated TiO₂ films compared to the reference TiO₂ film. This is consistent with the reduced V_{OC} values of the two plasmonic DSSCs as observed from their I–V characteristics (Table 2).

A similar shift in apparent Fermi level and a decrease in the photovoltage as has been reported for the DSSCs with silver nanoparticle-incorporated TiO₂ nanofibers [34] and for the case of single-crystal TiO₂ electrode that was deposited with thin Pt film [35].

3.6 Energy band gap from optical absorption spectra

The energy band gaps of reference TiO_2 powder as well as the TiO_2 powder incorporated with Au and Ag NPs were determined from UV–Vis absorption measurements as shown in Fig. 8. The E_g values are 3.26 eV for the reference TiO_2 powder, 3.14 eV for the TiO_2 -Au NP powder, and 3.01 eV for the TiO_2 -Ag NP powder, providing direct evidence for the band gap narrowing due to the presence of metal nanoparticles in TiO_2 .

3.7 EIS analysis

Figure 9 shows the Nyquist plots of the electrochemical impedance spectra of DSSCs with TiO_2 , TiO_2 -Au NP, and TiO_2 -Ag NP in the frequency range from 1×10^{-2} to 1×10^6 Hz. Each Nyquist plot in Fig. 8 displays two semicircles: the larger semicircle in the low-frequency range is related to the charge transport/accumulation at dye-attached TiO_2 /electrolyte interface resistance (R_{2CT}), and the smaller semicircle in high-frequency region is attributed to the charge-transfer resistance of the Pt counter electrode/electrolyte interface (R_{1CT}) [36, 37]. The impedance parameters were extracted using the equivalent circuit model (inset of Fig. 9), and the fitted lines are shown as solid lines in the Nyquist plots. The calculated values of the series resistance (R_s), charge-transfer resistance of the Pt/electrolyte interface (R_{1CT}) and charge-transfer resistance of the TiO_2 /electrolyte interface (R_{2CT}) based on the equivalent circuits for the three types of DSSCs are tabulated in Table 4.

As seen from Table 4, the R_s , R_{1CT} , and R_{2CT} values of the two plasmonic DSSCs are significantly lower

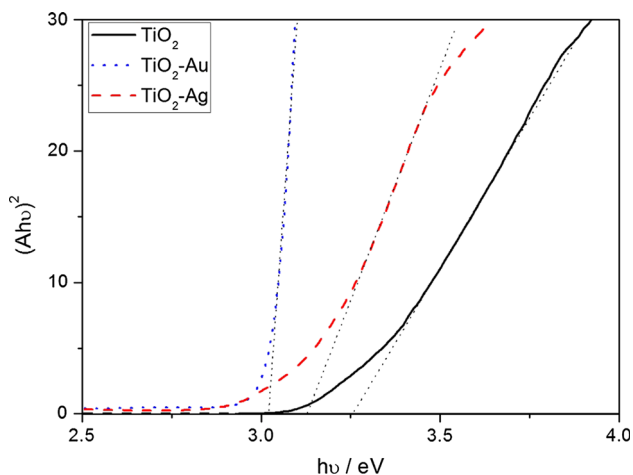


Fig. 8 Comparison of optical absorption curves for sintered powders, without dye for determination of the energy band gap values: (a) TiO_2 (b) TiO_2 -Au NP, and (c) TiO_2 -Ag NP. (Color figure online)

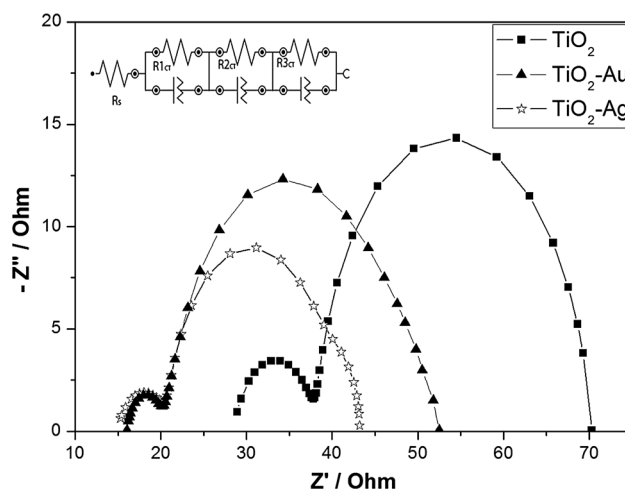


Fig. 9 Impedance plots taken for the three different DSSCs with TiO_2 , TiO_2 -Au NP, and TiO_2 -Ag NP in the frequency range of 1×10^{-2} – 1×10^6 Hz

than the corresponding quantities of the reference DSSC. The decrease in the R_{1CT} value of the NP-incorporated DSSCs is an indication of the increase in the oxidation rate of at the counter electrode and the redox mediator favoring the electron collection efficiency at the counter electrode. From the charge-transfer resistance values (R_{2CT}) in Table 4, one can see that the two plasmonic DSSCs exhibit lower resistance values implying more efficient charge-transfer processes across the TiO_2 metal NP/electrolyte interface, while the reference DSSC with TiO_2 shows the highest R_{2CT} . R_{2CT} has a value of 27.60 ohm for the reference cell, 6.08 ohm for the TiO_2 -Au NP cells, and 6.06 ohm for the TiO_2 -Ag NP cells indicating that the presence of metal NPs in TiO_2 in the two plasmonic DSSCs has improved the electron transport across the TiO_2 /electrolyte interface. This also contributes to the improved overall electron-transport process in the two plasmonic devices.

The results in Table 4 further show that the short-circuit current density J_{sc} of the three DSSCs increases with the decreasing R_{2CT} values in the order: TiO_2 , TiO_2 -Au NP, TiO_2 -Ag NP. The lower R_{2CT} values in the two plasmonic DSSCs clearly imply that by incorporating Au NP and Ag NPs into TiO_2 film, the electron-transfer mechanism at the TiO_2 /electrolyte interface has been improved. The better connectivity and more conducting pathways created by the presence of metal nanoparticles within the TiO_2 nanoporous structure (photoanode) is likely to facilitate this charge-transfer process, and it would be easier for the electrons released by the redox reaction at the interface to reach the dye cation across the Au/Ag TiO_2 electrode.

The Bode phase plots of EIS spectra, as shown in Fig. 10, display the frequency peaks of the charge-transfer process at the TiO_2 /electrolyte interface of the three DSSCs. The characteristic low-frequency peak f_{max} is

Table 4 Series resistance (R_s), charge-transfer resistance of the Pt/electrolyte (R_{1CT}), charge-transfer resistances of the TiO_2 /electrolyte (R_{2CT}) of DSSCs with TiO_2 , TiO_2 -Au NP, and TiO_2 -Ag NP

Cell configuration	J_{sc} ($mA\ cm^{-2}$)	V_{oc} (mV)	R_s (Ω)	R_{1CT} (Ω)	R_{2CT} (Ω)
(A) TiO_2	11.36	771.3	28.5	4.55	27.60
(B) TiO_2 -Au NP	12.00	737.3	15.3	3.88	6.08
(C) TiO_2 -Ag NP	13.86	729.1	14.9	3.65	6.06

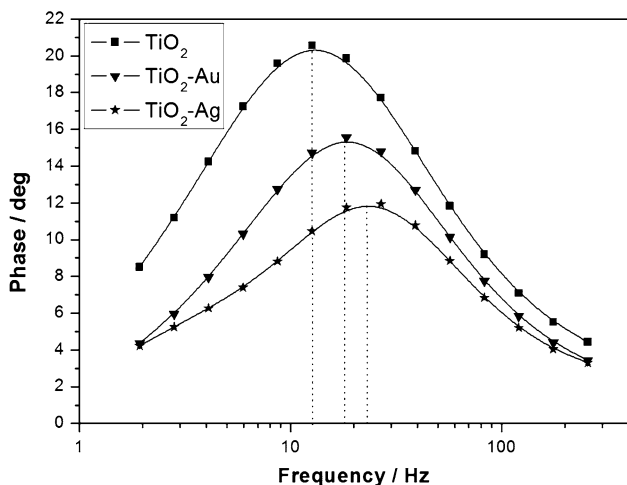


Fig. 10 Complex impedance data plotted as phase angle vs frequency (Bode Plots) for the three DSSCs with TiO_2 , TiO_2 -Au NP, and TiO_2 -Ag NP in the frequency range of 1×10^{-2} - 1×10^6 Hz

located at 12.73 Hz for the reference TiO_2 cell, at 18.14 Hz for the TiO_2 -Au NP cell, and at Hz for the TiO_2 -Ag NP cell. The electron lifetime (τ_r) in the DSSCs can be determined from the value of f_{max} [34]. Table 5 shows the relationship between V_{oc} , J_{sc} , and τ_r for the three types of DSSCs.

From Table 5, it can be seen that the electron life time τ_r is highest for the reference cell A (TiO_2), and the V_{oc} of this cell is also the highest. τ_r values of Au NP and Ag NP-incorporated cells (B and C) are significantly lower, and their V_{oc} values are also lower compared to the reference cell A (TiO_2). Shorter electron life time means faster recombination. Therefore, the presence of Au and Ag nanoparticles in TiO_2 in the two plasmonic DSSCs can promote nonradiative recombination either with dye cations or with I_3^- redox species leading to a reduced number of electrons arriving at the collecting electrode.

Table 5 Electron recombination life times (τ_r), extracted from the Bhode plots (Fig. 7)

DSSC anode	η %	F_{max} (Hz)	τ_r (ms)	J_{sc} ($mA\ cm^{-2}$)	V_{oc} (mV)
(A) TiO_2 -dye	5.12	12.73	12.50	11.36	771.3
(B) TiO_2 -Au NP -dye	6.23	18.14	8.77	12.00	737.3
(C) TiO_2 -Ag NP -dye	6.51	23.09	6.89	13.86	729.1

The reduction in V_{oc} of the two plasmonic DSSCs might be related to the increased electron recombination. However, the enhancement in J_{sc} surpasses the drop in V_{oc} so that the net result has been the enhancement in efficiency. Very similar results, namely, decreases in τ_r and V_{oc} for Ag NP-incorporated TiO_2 nanofiber-based DSSCs have been reported by Li et al. [34].

3.8 Dark I-V analysis

Comparison of dark I-V characteristics for the three DSSCs based on TiO_2 , TiO_2 -Au NP, and TiO_2 -Ag NP is shown in Fig. 11. The onset under reverse bias occurs at three different voltages for the three cells as shown in Table 6.

Interfacial electron-transfer processes are central for the working principle of the DSSC device. In a typical DSSC

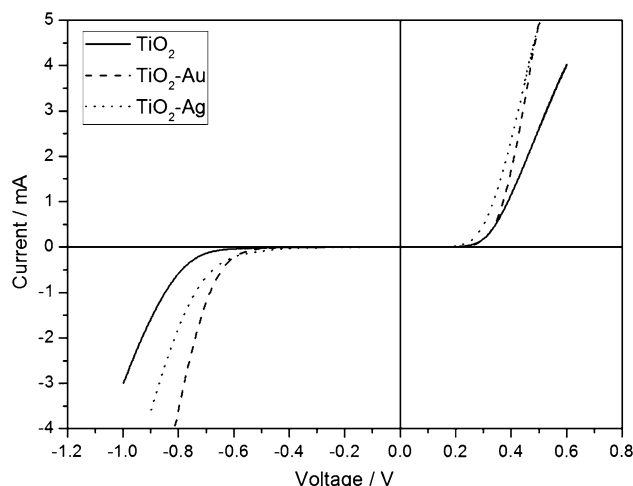


Fig. 11 Dark I-V characteristics of the three DSSCs with TiO_2 , TiO_2 -Au NP, and TiO_2 -Ag NP photoanodes

Table 6 Onset of the reverse breaking voltages of the three DSSCs with three different photoanodes

DSSC anode	Reverse breaking down voltage (onset) (mV)	V_{oc} (mV)
(A) TiO ₂ -dye	−579	771.3
(B) TiO ₂ -Au NP -dye	−502	737.3
(C) TiO ₂ -Ag NP -dye	−487	729.1

under illumination, the following processes occur: (a) Dye excitation, (b) Electron injection, (c) Electron recombination with dye cations, (d) Electron recombination with redox electrolyte, and (e) Dye regeneration. The recombination with redox species in the electrolyte ((d) above) is often referred to as dark current, as it is essentially independent of light. In contrast, the recombination pathway to the oxidized dye requires light and does not occur in the dark. The charge recombination at the TiO₂-redox electrolyte interface is expected to play a significant role in lowering the photovoltage. The V_{oc} value kinetically manifests the degree of back electron transfer from the TiO₂ conduction band to the I_3^- ions in the electrolyte. The recombination of TiO₂ conduction band electrons with the holes in the electrolyte, i.e., I_3^- , is the most significant loss mechanism in a DSSC [38, 39].

The dark current measurement of DSSCs provides a qualitative measure for the current leakage due to the back electron transfer. In a typical DSSC, the origin of the dark current stems from the existence of naked FTO sites due to the porous nature of the TiO₂ structure. The porous structure provides pathways for the commonly used liquid redox electrolyte (e.g., I_3^- species) to penetrate through the TiO₂ film and contact the bare conductive FTO surface. At these bare sites, the potential is thermodynamically favorable for the reduction of the oxidative species, mainly I_3^- . This causes electron recombination and results in the loss of photovoltage.

In general, in a typical DSSC, the electron back injection from the conduction band of TiO₂ to electrolyte is due to trapping of conduction band electrons by deep states followed by reduction processes at the interface. In a plasmonic DSSC, this process is facilitated due to the presence of metal nanoparticles in the TiO₂ matrix and due to the lower charge-transfer resistance, R_{2CT} . In a plasmonic DSSC, there are more recombination pathways within the TiO₂ semiconductor due to the presence of metal NPs which could provide additional transient sites for electron migration. The rate of recombination or the rate of reaction of I_3^- ions with the electrons at the surface of the dyed TiO₂ electrode will increase with the conduction band electron concentration resulting in back current and the accompanying decrease of the open-circuit voltage. In the

present study, higher electron concentration in the composite TiO₂ electrode (TiO₂ semiconductor with Au or Ag nanoparticles) would lead to a higher back current in the two plasmonic DSSCs compared to the reference DSSC.

As seen from Fig. 11 and Table 6, the breakdown voltages at the negative region in the two plasmonic DSSCs are lower compared with the reference DSSC indicating that the electron recombination of the plasmonic DSSCs is greater. This indicates that the rate of the reaction of I_3^- with electrons at the surface of the dyed TiO₂ electrode is greater for the two plasmonic DSSCs, leading to a reduction in their V_{OC} value. This is consistent with the lower electron lifetimes derived from EIS measurements for the two plasmonic DSSCs as discussed earlier. The reduced V_{OC} , of course, will make a negative contribution to the observed efficiency enhancement in the two plasmonic DSSCs [40]. Similar results have been reported by Li et al. for plasmonic DSSCs fabricated with Ag NP-incorporated TiO₂ nanofiber-based photoanodes [34].

It should be mentioned that, our initial attempts were focused on incorporating a mixture of Au NPs and Ag NPs in different molar ratios, to benefit from the wider spectral range seen in the optical absorption spectrum. However, despite many attempts, the efficiencies of the corresponding plasmonic DSSCs were lower than the DSSC with pristine TiO₂. One could speculate that, this could possibly be due to a destructive interference effect resulting from the two resonance plasma frequencies.

4 Conclusion

plasmon-enhanced energy conversion in DSSCs with Au- and Ag NP-modified TiO₂ photoanode has been investigated. It was observed that the efficiency of the plasmonic DSSCs for a selected size range of nanoparticles depends strongly on the added amount of Au and Ag NPs. For each plasmonic cell, the efficiency showed a maximum with the increasing amount of NPs. Compared with the normal DSSC with pristine TiO₂ photoanode, the short-circuit current density (J_{sc}) and the fill factor (FF) of the DSSCs with Au and Ag NP-incorporated TiO₂ electrode were improved, enhancing the overall solar cell efficiency by 21.6 % for the Au NPs and 27.1 % for the Ag NPs. Based on consistent results from several types of electrochemical and optical measurements, it is clear that the Au- and Ag NP-incorporated plasmonic DSSCs exhibit two processes: (a) high optical absorption characterized by a red shift in the IPCE max peak and a significantly-enhanced optical absorption induced by the surface plasmon resonance effect, enhancing the short-circuit current density, J_{sc} and the efficiency; and (b) low open-circuit voltage, V_{oc} resulting from the narrowing of the energy band gap due to

the presence of metal NPs in TiO₂ and the reduced electron life times increasing the electron recombination with redox species at the TiO₂/electrolyte interface.

Acknowledgments Authors wish to thank Dr. LP Teo and the Centre for Ionics, University of Malaya (CIUM) for carrying out the XRD measurements.

References

- O'Regan B, Grätzel M (1991) A low-cost, high-efficiency solar cell based on dye-sensitized colloidal TiO₂ films. *Nature* 353:737–740
- Hara K, Arakawa H (2003) Dye-sensitized solar cells. In: Tachibana Y, Hara K, Sayama K, Arakawa H (eds) *Handbook of photovoltaic science and engineering*. John Wiley & Sons Ltd, Chichester, pp 664–670
- Koumura N, Wang Z, Mori S, Miyashita M, Suzuki E, Hara K (2006) Alkyl-functionalized organic dyes for efficient molecular photovoltaics. *J Am Chem Soc* 128:14256–14257
- Grätzel M (2005) Solar energy conversion by Dye-sensitized photovoltaic cells. *Inorg Chem* 44:6841–6851
- Dissanayake MAKL, Thotawatthage CA, Senadeera GKR, Bandara TMWJ, Jayasundera WJMJSR, Mellander B-E (2012) Efficiency enhancement by mixed cation effect in dye-sensitized solar cells with PAN based gel polymer electrolyte. *J Photochem Photobiol A* 246:29–35
- Wang H, Zhang X, Gong F, Zhou G, Wang Z (2012) Novel ester-functionalized solid-state electrolyte for highly efficient all-solid-state dye-sensitized solar cells. *Adv Mater* 24:121–124
- Dissanayake MAKL, Rupasinghe WNS, Seneviratne VA, Thotawatthage CA, Senadeera GKR (2014) Optimization of iodide ion conductivity and nano filler effect for efficiency enhancement in polyethylene oxide (PEO) based dye sensitized solar cells. *Electrochim Acta* 145:319–326
- Nazeeruddin M, Kay A, Rodicic I, Humphry-Baker R, Müller E, Liska P (1993) Conversion of light to electricity by cis-XzBis(2,2'-bipyridyl-4,4'-dicarboxylate)ruthenium(II) charge-transfer sensitizers (X = Cl-, Br-, I-, CN-, and SCN-) on nanocrystalline TiO₂ electrodes. *J Am Chem Soc* 115:6382–6390
- Dissanayake MAKL, Divarathne HKDMNR, Thotawatthage CA, Dissanayake CB, Senadeera GKR, Bandara BMR (2014) Dye-sensitized solar cells based on electrospun polyacrylonitrile (PAN) nanofibre membrane gel electrolyte. *Electrochim Acta* 130:76–81
- Chandrasekharan N, Kamat P (2000) Improving the photoelectrochemical performance of nanostructured TiO₂ films by adsorption of gold nanoparticles. *J Phys Chem B* 104:10851–10857
- Standridge S, Schatz G, Hupp J (2009) Distance dependence of plasmon enhanced photocurrent in dye-sensitized solar cells. *J Am Chem Soc* 131:8407–8409
- Ding K, Zhu J, McGehee M, Cai W, Moon S, Cai N et al (2011) Plasmonic dye-sensitized solar cells. *Adv Energy Mater* 1:52–57
- Zhang DZ, Wang M, Brolo A, Shen J, Li X, Huang S (2013) Enhanced performance of dye-sensitized solar cells using gold nanoparticles modified fluorine tin oxide electrodes. *J Phys D Appl Phys* 46:024005–024013
- Meen T, Tsai J, Chao S, Lin Y, Wu T, Chang T (2013) Surface plasma resonant effect of gold nanoparticles on the phototransistors of dye-sensitized solar cells. *Nanoscale Research Lett* 8:450–456
- Jeong N, Prasittichai C, Hupp J (2011) Photocurrent enhancement by surface plasmon resonance of Silver nanoparticles in highly porous dye-sensitized solar cells. *Langmuir* 27(23):14609–14614
- Ihara M, Tanaka K, Sakaki K, Honma I, Yamada K (1997) Enhancement of the absorption coefficient of cis-(NCS)2 Bis(2,2'-bipyridyl-4,4'-dicarboxylate)ruthenium(II) dye in dye-sensitized solar cells by a silver Island film. *J Phys Chem B* 101:5153–5157
- Jeong NC, Prasittichai C, Hupp J (2011) Photocurrent enhancement by surface plasmon resonance of silver nanoparticles in highly porous dye-sensitized solar cells. *Langmuir* 27:14609–14614
- Ding IK, Zhu J, Cai W, Moon SJ, Cai N, Wang P, Zakeeruddin S, Grätzel M, Brongersma MML, Cui Y, McGehee MD (2011) Plasmonic dye-sensitized solar cells. *Adv Energy Mater* 1:52–57
- Hou W, Pavaskar P, Liu Z, Theiss J, Aykol M, Cronin SB (2011) plasmon resonant enhancement of dye-sensitized solar cells. *Energy Environ Sci* 4:4650–4655
- Chang S, Li Q, Xiao X, Wong KY, Chen T (2012) Enhancement of low energy sunlight harvesting in dye-sensitized solar cells using plasmonic gold nanorods. *Energy Environ Sci* 5:9444–9448
- Zhang X, Liu J, Li S, Tan X, Yu M, Du J (2013) Bioinspired Synthesis of Ag@TiO₂ plasmonic nanocomposites to enhance the light harvesting of dye-sensitized solar cells. *RSC Adv* 3:18587–18595
- Chang H, Chen C, Kao M, Hsiao H (2014) Effect of core-shell Ag@TiO₂ volume ratio on characteristics of TiO₂-based DSSCs. *J Nanomater* 2014:264108–264116
- Brown M, Suteewong T, Kumar R, D'Innocenzo V, Petrozzo A, Lee M (2011) Plasmonic dye-sensitized solar cells using core-shell metal-insulator nanoparticles. *Nano Lett* 11:438–445
- Sheehan S, Noh H, Brudvig G, Cao H, Schmuttenmaer C (2013) Plasmonic enhancement of dye-sensitized solar cells using core-shell nanostructures. *J Phys Chem C* 117:927–934
- Tabrizi A, Ayhan F, Ayhan H (2009) Gold nanoparticle synthesis and characterisation. *Hacettepe J Biol Chem* 37(3):217–226
- Huang H, Yang X (2003) Chitosan mediated assembly of gold nanoparticles multilayer. *Coll Surf A* 226:77–86
- Chang H, Chen D (2009) Fabrication and photocatalytic activities in visible and UV light regions of Ag@TiO₂ and NiAg@TiO₂ nanoparticles. *Nanotechnology* 20:105704–105714
- Ratyakshi I, Chauhan R (2009) Colloidal synthesis of Silver Nanoparticles. *Asian J Chem* 21(10):113–116
- Njoki PN, Lim IIMS, Mott D, Park HY, Khan B, Mishra S, Sujakumar R, Luo J, Zhong CJ (2007) Size correlation of optical and spectroscopic properties for gold nanoparticles. *J Phys Chem C* 111:14664–14669
- Eustis S, El-Sayed NA (2006) Why Gold Nanoparticles are more precious than pretty gold: noble metal surface plasmon resonance and its enhancement of the radiative and nonradiative properties of nanocrystals of different shapes. *Chem Soc Rev* 35:209–217
- Hagglund C, Zach M, Kasemo B (2008) Enhanced charge carrier generation in dye sensitized solar cells by nanoparticle plasmons. *Appl Phys Lett* 92:013113–013113
- Chandrasekharan N, Kamat P (2000) Improving the Photoelectrochemical Performance of Nanostructured TiO₂ Films by Adsorption of Gold Nanoparticles. *The J Phys Chem B* 104(46):10851–10857
- Rand B, Peumans P, Forrest S (2004) Long-range absorption enhancement in organic tandem thin-film solar cells containing silver nanoclusters. *J Appl Phys* 96:7519–7526
- Li J, Chen X, Ai N, Hao J, Chen Q, Strauf S (2011) Silver nanoparticle doped TiO₂ nanofiber dye sensitized solar cells. *Chem Phys Lett* 514:141–145
- Nakato Y, Shioji M, Tsubomura H (1982) Photoeffects on the potentials of thin metal films on a n-TiO₂ crystal wafer The mechanism of semiconductor photocatalysts. *Chem Phys Lett* 90:453–456
- Subramanian V, Wolf E, Kamat PV (2001) Semiconductor – metal composite nanostructures. to what extent do metal

- nanoparticles improve the photocatalytic activity of TiO₂ films. *J Phys Chem B* 105(46):11439–11446
37. Pan M (2013) Enhanced efficiency of dye-sensitized solar cell by high surface area anatase-TiO₂-modified P25 paste. *J Nanomater* 2013:760685–760691
 38. Park NG, Lagemaat JVD, Frank AJ (2000) Comparison of dye-sensitized rutile and anatase-based TiO₂ solar cells. *J Phys Chem B* 104:8989–8994
 39. Tang Xiao, Wang Yuxun, Cao Guozhong (2013) Effect of the adsorbed concentration of dye on charge recombination in dye-sensitized solar cells. *J Electroanal Chem* 694:6–11
 40. Sathiya Priya AR, Subramania A, Jung Young-Sam, Kim Kang-Jin (2008) High-performance quasi-solid-state dye-sensitized solar cell based on an electrospun PVdF-HFP membrane electrolyte. *Langmuir* 24(17):9816–9819